I-V Characteristics of III-V Compounds (GAAS) for MOSFET Devices

S.S. AL-AMEER and F. ALMARZOUKI
Faculty of Science, Physics Department,
King Abdulaziz University, Jeddah, Saudi Arabia

ABSTRACT. A new approach of examining and characterizing both thin film or thin film based devices are described in this paper. Justification of the selected techniques which have been utilized in fabricating these thin films are given. The important aspect of selecting the substrates on which the thin films are made were pointed out. The measurement techniques which have been adopted here are discussed. Results and discussion show the ability, reliability and simplicity of these proposed techniques. The results are interesting and confirm the method used to produce them, even though it is an oil pumped system.

Introduction

In thin films and/or thin film devices the thickness is appreciably reduced so that the forces acting upon a particle existing at or near its surface are substantially different from those acting on particle existing in the internal volume. This is not the case with conventional bulk bodies where the forces acting upon all particles are equal. The existence of surface defects which disturb the energy band structure at the surface, affect the interaction between the very close surfaces of a thin film[1,2].

Thin film physics and its technology have been greatly developed in the last ten years[2,3] in order to meet the pressing need for scaling down the dimensions of electronic equipment. This has been stimulated by space exploration with its demand for intricate radioelectronic equipment's of high reliability, and small size and weight.

2. Fabrication Technique

2.1. Vacuum Evaporation

This is the most widely used method for thin film preparation. It is simple and can under proper conditions, provide films of extreme purity. It can also, to a certain extent,

achieve a pre-selected structure. The formation of thin films by this method proceeds as follows[3,4]:

1. Transformation of the material to be deposited by evaporation into gaseous state.
2. Transfer of the vapor atoms or molecules from the evaporation source to the substrate.
3. Deposition of these particles on the substrate.
4. Rearrangement or modification of their binding on the substrate surface.

2.2 Vacuum Evaporation Techniques

This section overviews the apparatus, the substrate preparation, the important materials for evaporation and the evaporation sources.

a) Apparatus

The apparatus should meet some special requirements:

1. Sufficiently low threshold pressure.
2. Sufficiently fast achievement of this pressure from atmospheric gauge.
3. Easily accessible working chamber.
4. Working chamber uncontaminated by organic vapors.

The first two requirements necessitate the use of high-vacuum pumps with sufficient pumping needs and the shortest and widest possible piping between the pump and the exhausted space. Metal-oil diffusion pumps with high quality silicon oil are used and pre-exhausted by a rotary pumps. The penetration of oil vapors into the working chamber is prevented by creating cooled zones (with liquid nitrogen or water) above the pump, where the oil vapor is trapped. A valve is placed between the pump and the exhausted chamber to shorten the working cycle.

As shown in Fig. (1), the working chamber consists of a bell jar (metal or glass) manually or hydraulically mounted. The lower part acts as a collar with many feedthroughs (electrical and mechanical) and connections for a vacuum gauge thickness monitor. In addition, it is equipped with a needle valve for controlling the gas inlet.

A liquid nitrogen trap is used to realize 10^{-4} to 10^{-6} torr vacuum by the initial adsorption of the atmospheric pressure gases.

b) Substrate

The substrate serves as a mechanical support and insulator (high dielectric strength). It should be chemically passive in order not to change the film properties. It must provide adequate adhesion of the film to its surface during the high temperature operation. To ensure a constant temperature of surface during deposition, it should have a sufficient heat removal capability. Further, it should be flat and smooth to guarantee defined and reproducible properties.

The most widely used substrates for polycrystalline film are glass, fused silica, and ceramics. For a single-crystal growth to be realized, single-crystal silicon, alkali halide, or mica substrates should be used.

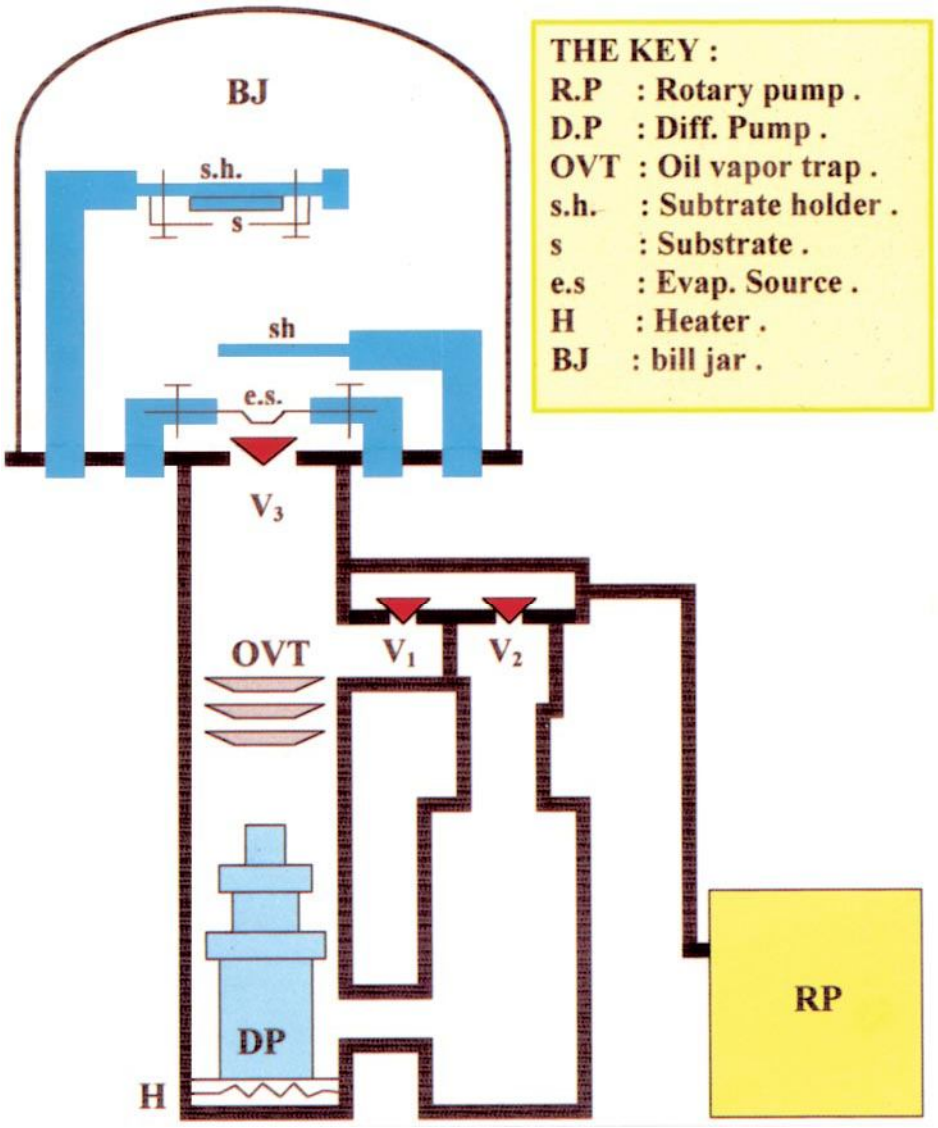

FIG. 1. Layout of vacuum evaporation system.

The substrate should be absolutely clean and uncontaminated. To fulfill this condition without causing mechanical or chemical damage by abrasive substances or strong chemicals, it is recommended to proceed as follows: Application of ultrasound in a solution of ionic detergent through rinsing in deionized distilled water, degreasing in a vapor of pure alcohol and finally drying in a stream of dry and filtered nitrogen. Better results can be achieved if the substrate is heated, afterwards, in vacuum to a temperature of 300ºC.

The substrate may be heated during deposition by a tungsten, tantalum or nichrome filament. A thermocouple may be deposited on the substrate and used to measure its temperature during vacuum processing.

c) Evaporation Materials

Pure metals (Ag, Al), III-V compound, semiconductors (GaAs) are examples of evaporants used. The evaporant temperature should be raised to the adequate value corresponding to the saturated vapor pressure (~10^{-6} to 10^{-2}) which is usually given in tables.

To avoid contamination arising from the layers of chemical compounds formed on the surface of evaporants, the substrate is shielded by a shutter at the beginning of the evaporation.

To avoid contamination with the source material it is also recommended not to evaporate all the substrate from the source by the end of evaporation.

d) Evaporation Sources

These sources are made of high melting point metals (Ta, Mo). They are used in the form of wires, foils or boats. The evaporate material is contained in a boat, having been powdered in a crucible, surrounded by a spiral heater or wound or hung on the source wire.

3. Device Construction

The H.V. system has been used to evaporate the material in which GaAs was used. Controlling the film thickness was not very important but by using a film thickness monitor we were able to evaporate 3000 to 4000 Å layers. Two types of pumps have been used with an Edwards-5 two stage rotary pump connected to the E04-liquid nitrogen baffled oil diffusion pump. These two pumps can achieve together a pressure of about 10^{-6} mbar which is low enough for our device purposes. After this all the films are covered by a mechanical mask except the gate effective area shown in Fig. (2). Then the sample is mounted into the evacuated furnace and the unmasked area is exposed to pure oxygen under a different temperature, but at fixed oxidation time and pressure. The sample is then transferred to the vacuum system and a thin metal contact deposited on the top of the oxide layer. An approximate estimation of the oxide layer is about 400-500 Å[4-5]. Silver paint is used for the electrical measurements.

4. Measurement Techniques

Electrical contacts to the films were made by connecting 0.25 mm copper wire using air dried silver paint. The electrical contact arrangements are shown in Fig. (3a, 3b). A schematic diagram of the experimental set-up is shown in Fig. (4) where a programmable pico

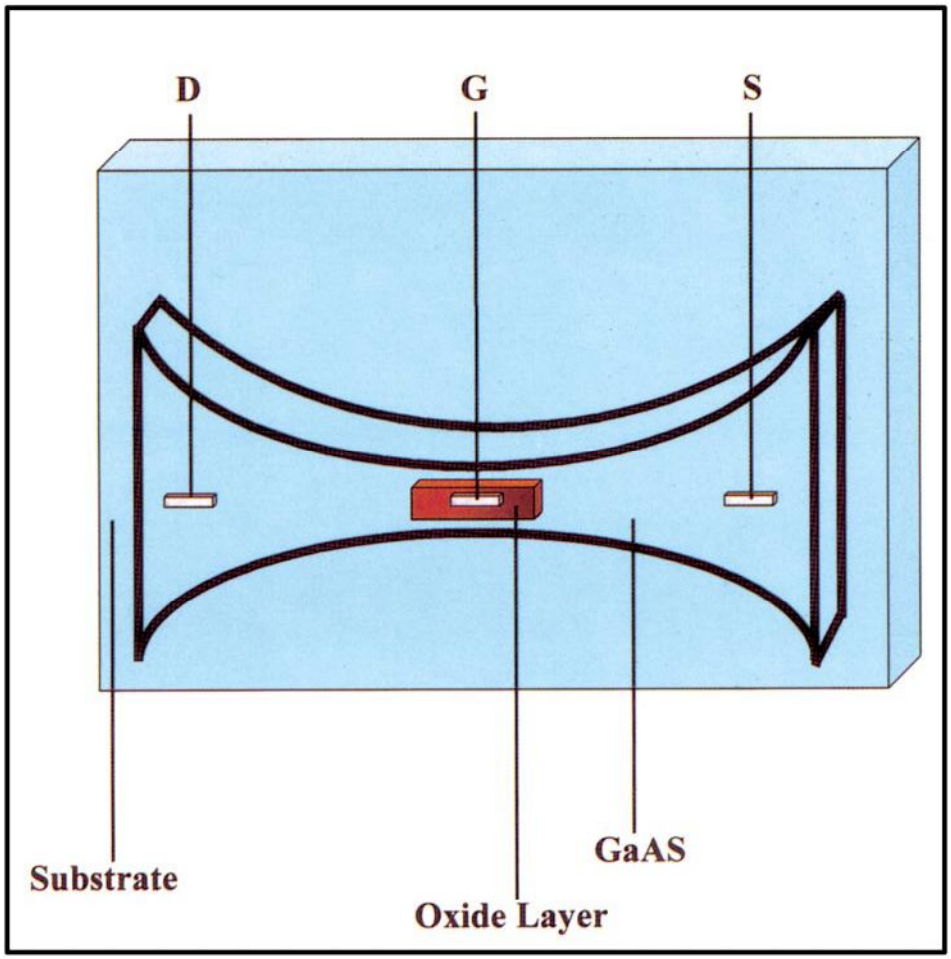

FIG. 2. Configuration of the sample of GaAs with channel gate (Mos devices).

Ameter (HP4140B), control box, oscilloscope, and x-y recorder have been used. Since the device current to be measured is very small, accurate measurements were undertaken using the smallest range of the pico Ameter (ranging from 10^{-10} to 10^{-12}A). We have found that it was very difficult to plot the device performance on the x-y plotter easily, and instead point by point measurements were the most suitable method. However both methods have been adopted successfully.

5. Result and Discussion

The starting material was CERAC grade GaAs with 99.999% purity and fine grain size. Thermal deposition was, in general, on the glass substrate with deposition rates of the order of 10Å/sec. at room temperature. X-ray examination showed a polycrystalline structure[8,9].

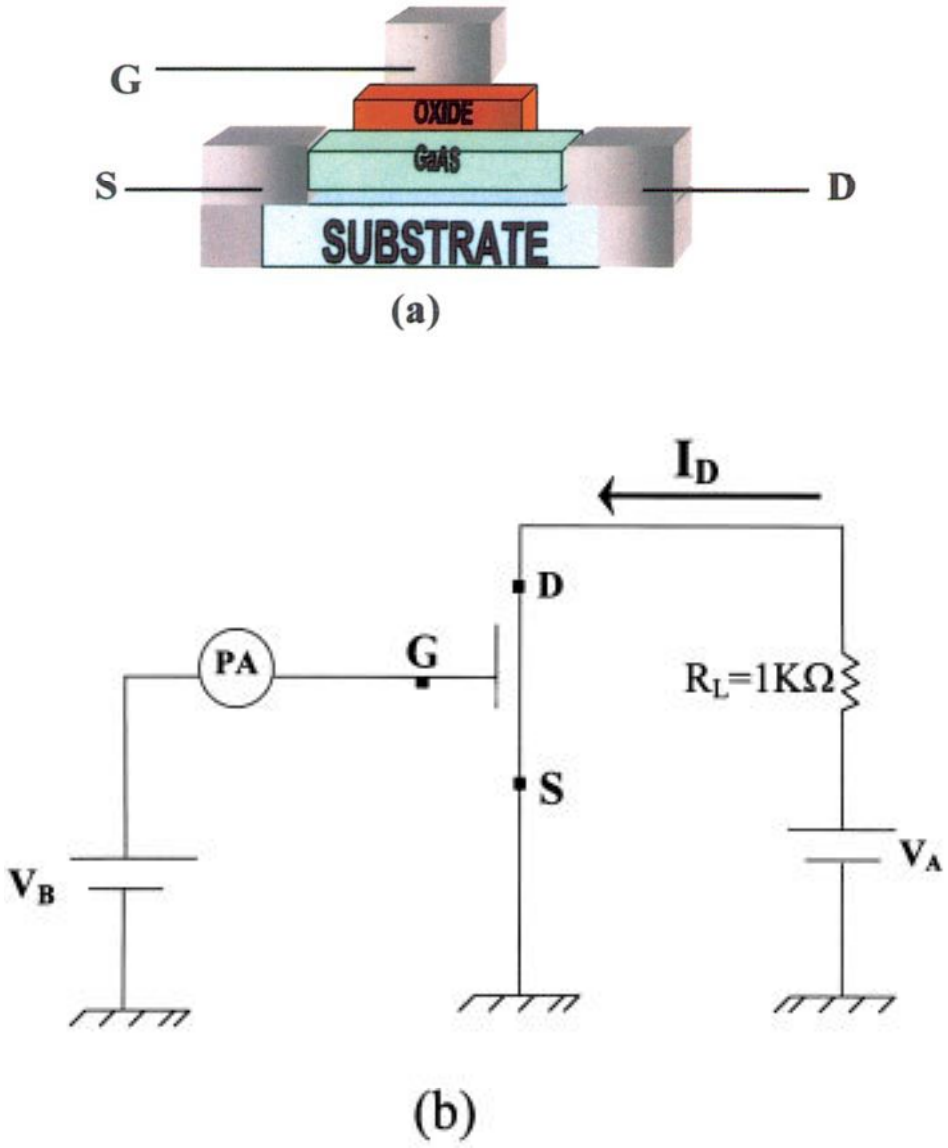

FIG. 3(a,b). Sample and electrical circuit.

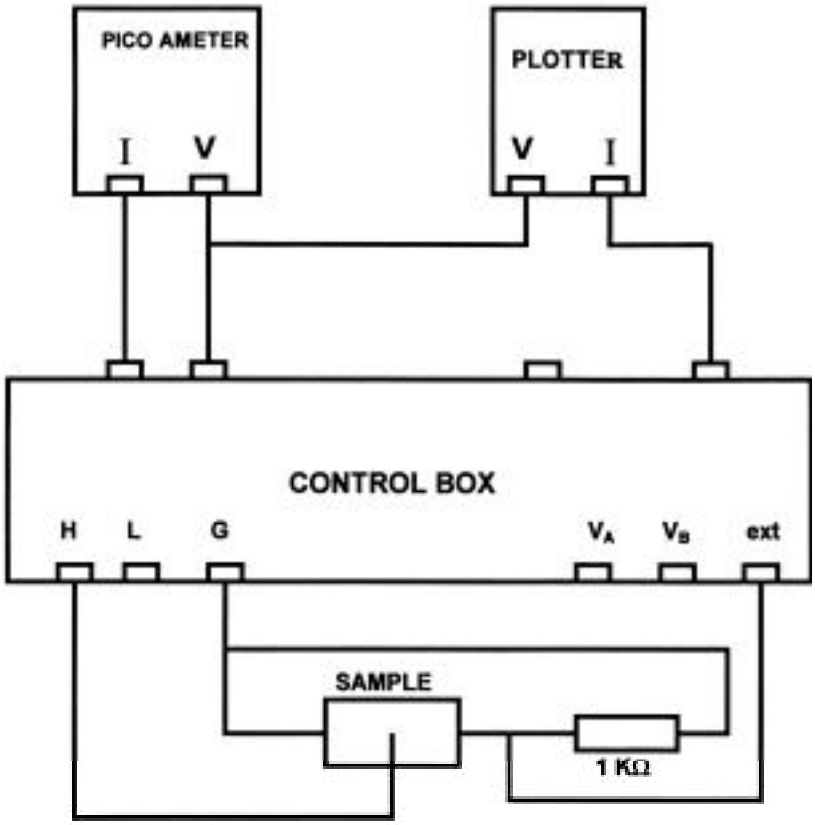

FIG. 4. Block diagram of electrical measurements.

Measurements have been carried out on several thin films which were prepared using the evaporation techniques. The I-V curve of these films are shown in Fig. (5). These measurements have been repeated many times and it was found that up to 200ºC annealing temperature, there is no effect on the ohmic straight line of the I-V curve. Increasing the annealing temperature from 250-350ºC at least 3-4 out of five times, similar displays of I-V characteristics were found.

The effect of substrate annealing at different temperatures under vacuum has indicated that the quality of the device is substantially changing from the ohmic region of the saturated region as shown in Fig. (6) even though, the oxidation pressure and time are kept constant for all the experimental runs. Table (1) shows the measured values of the deposition parameter as well as the electric properties of the GaAs films.

6. Conclusion

Our study shows the effect of the temperature on the behaviour of the I-V characteristics, in which for high temperature with the same pressure and oxidation time the re-

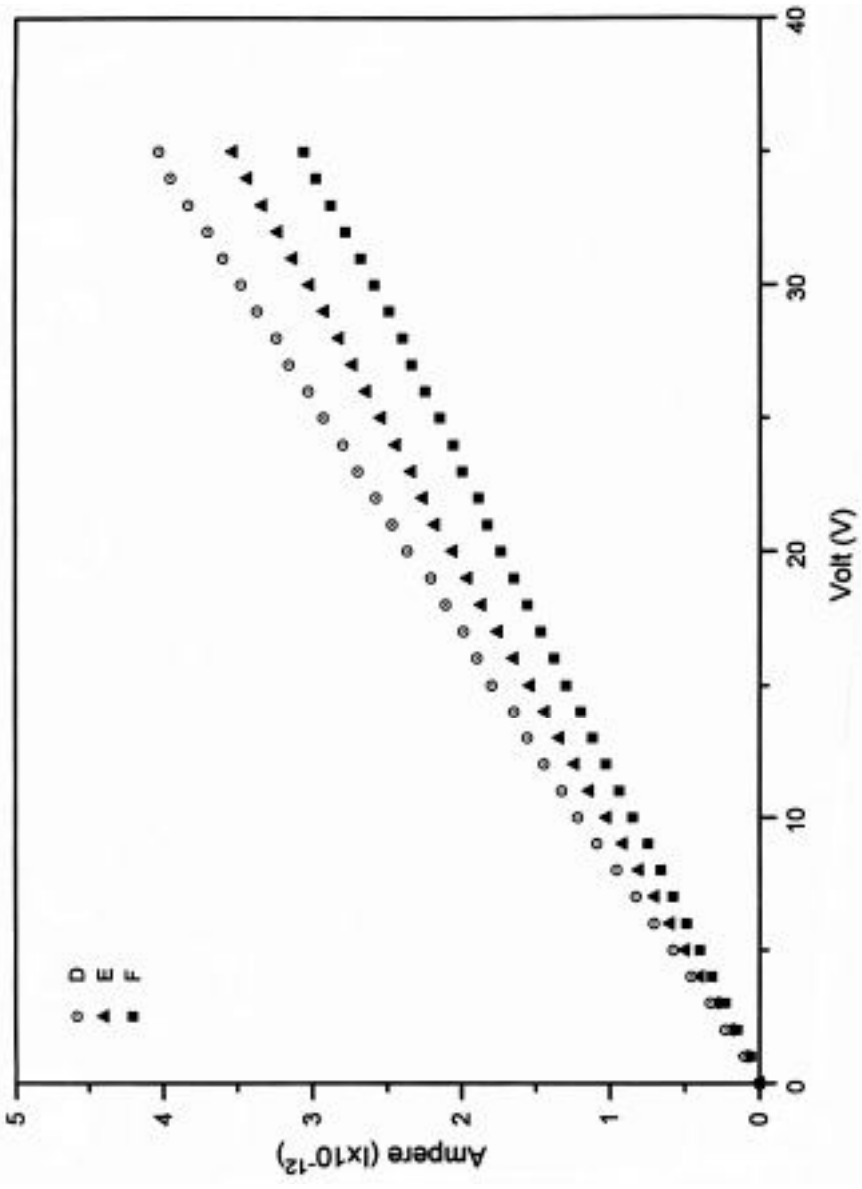

FIG. 5. Comparison of the I-V Characteristics for III-V Compounds GaAs Sample D, T = 200 ºC, P = 25 mbar, Time = 1 hour, Sample E, at T = 150 C, P = 25 mbar, Time = 1 hour, Sample F, T = 100 ºC, P = 25 mbar, Time = 1 hour.

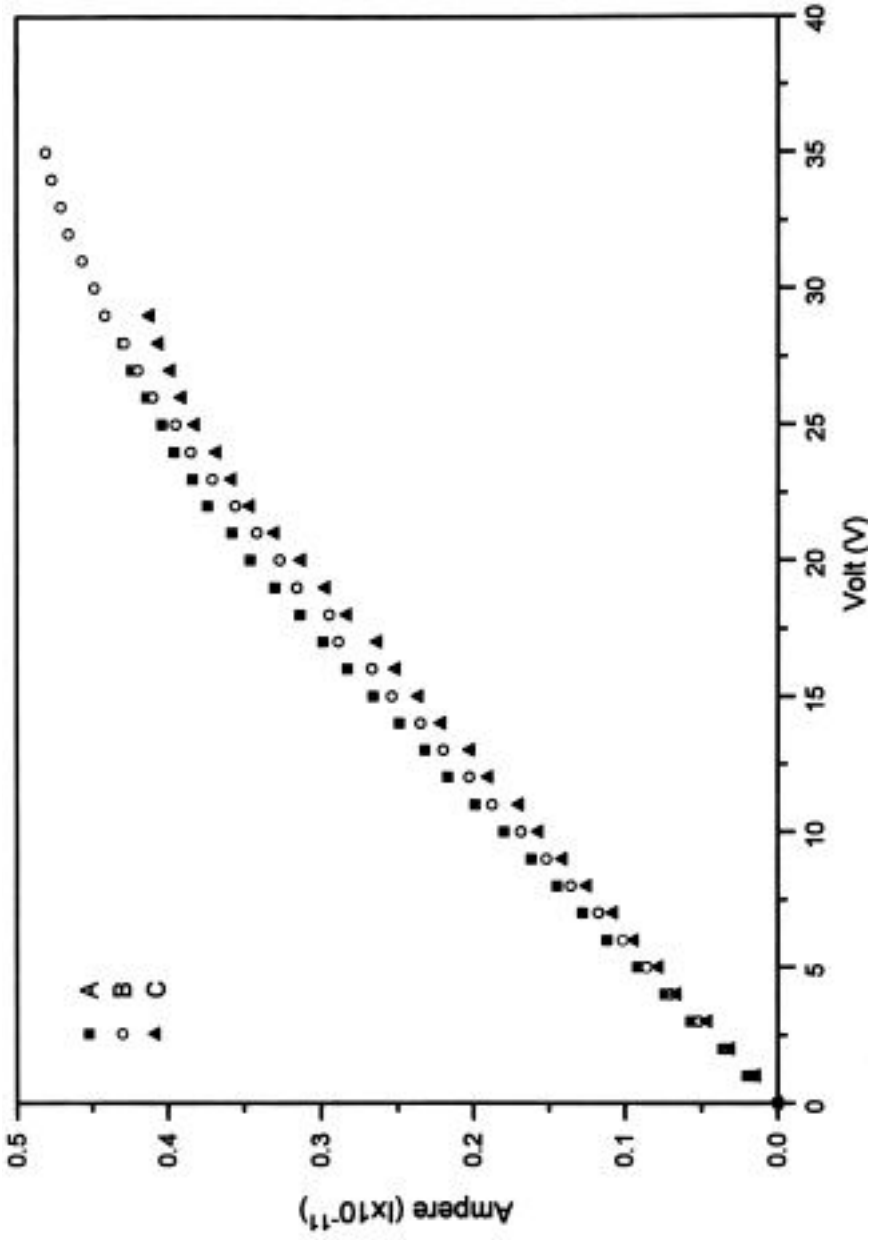

FIG. 6. Comparison of the I-V Characteristics for III-V Compounds GaAs Sample A, T = 350 ºC, P = 25 mbar, Time = 1 hour, Sample B, T = 300 C, P = 25 mbar, Time = 1 hour, Sample C, T = 250 ºC, P = 25 mbar, Time = 1 hour.

action between the O_2 and III-V increase[10] substantially, while at room temperature, the reaction does not affect the device. Our result shows this phenomenon for many devices and is reproducible.

TABLE 1. Comparison between the electronic parameter for three samples of GaAs films at different temperatures.

Film no.	T°C	P mbar	Time hour	$\rho \times 10^{7}$ Ω - cm	$\sigma \times 10^{-8}$ Ω^{-1} cm^{-1}	η_i cm^{-3}	μ cm^2/ v-sec	$I_{ave} \times 10^{-11}$ A	J $\times 10^{-9}$ A/cm^2	E v/cm
A	350	25	1	2.29	4.37	3.25	8404	0.17	0.68	0.016
B	300	25	1	2.44	4.098	3.25	7881	0.16	0.64	0.016
C	250	25	1	2.54	3.94	3.25	7577	0.15	0.6	0.015

This device can be used in many applications in the field of the MOS transistors, which has the advantage of extremely high input impedance on the gate channel. This impedance can be of the order 10^{15} Ω, making this device very useful for amplification purposes. Also these devices are very useful in integrated circuits in general.

References

[1] **Heavens, O.S.,** *Thin Film Physics,* John Wiley & Sons Inc., New York, 152 p. (1973).

[2] **Razik, N., Al-Barakati, G.** and **Al-Heneti, S.,** Refinement of GaAs Powder Diffraction Data, *J. Matter. Sci. Lett.,* pp. 1458-1460 (1989).

[3] **Stuart, R.V.,** *Vacuum Technology, Thin Film and Sputtering,* Academic Press, Paris, 266 p. (1983).

[4] **Sze, S.M.,** *Physics of Semiconductor Devices,* John Wiley & Sons, Inc., New York, 868 p. (1981).

[5] **Webb, P.W.,** Thermal Modeling of Power GaAs Microwave IC's, *IEEE Tran. Elec. Dev.,* **40**(5): 867-877 (1993).

[6] **Hass, G., Francombe, M.H.** and **Hoffman, R.W.** (eds.), *Physics of thin films, Advances in Research and Development,* Vol. **7,** Academic Press, New York and London, pp. 43-111 (1973).

[7] **Hass, G.** (ed.), *Physics of Thin Films, Advances in Research and Development*, Vol. **1,** Academic Press, New York and London, pp. 123-184 (1963).

[8] **Wong, H.** and **Cheng, Y.,** Modeling of Low-Frequency Noise in MOSFET with Electron Trapping Detrapping at Oxide-Silicon Interface, *IEEE Trans. on Elec. Dev.,* **30**(8): 1883-1888 (1991).

[9] **Wouters, D.J., Colinge, J.P., Mass, H.E.,** Subthreshold Current in Thick and Thin Film SOI MOSFET, *Transistors Proc., IEEE SOS/SOI Techno Conf. IEEE, IEEE Service Center, USA,* **1:** 21-22 (1989).

[10] **Reichelt, K., Jiang, X.,** The Preparation of Thin Films by Physical Vapour Deposition Methods, *Thin Solid Films,* **191:** 91-126 (1990).

علاقـة التيار بالجهد للمركبا (III - V) لمادة الجاليوم أرسنيد المستخدم لوصلا الـ - MOSFET

سعيد سعد الأمير و فهد مسعود المرزوقي
قسم الفيزياء ، كلية العلوم ، جامعة الملك عبد العزيز
جـــدة – المملكة العربية السعودية

المستخلص . في هذا البحث تم اتباع طريقة بحثية مبسطة لفحص ونمذجة الأغشية الرقيقة المنتجة بواسطة أجهزة التفريغ وقد تم اختيار تقنية مبسطة جداً لفحص هذه الأغشية والتي عملت على شكل أغشيةرقيقة فقط وأغشية على شكل دوائر إليكترونية . وهذه التقنية عبارة عن استخدام جهاز بيكوأميتر *(HP 4140)* وملحقاته وكانت النتائج في غاية الأهمية من ناحية التطبيقا الإليكترونية سواء في مجال المكبرا أو مجال الدوائر المتكاملة .

Measurement of Neutron Flux at the NSCL K1200 Cyclotron for 80 MeV/u $^{18}O^{6+}$ Beam on a ^{9}Be Target

SALEM ALI SALEM SHAHEEN*
Department of Physics, Faculty of Science,
King Abdulaziz University, Jeddah, Saudi Arabia

ABSTRACT. The neutron flux at the NSCL K1200 cyclotron accelerator target at the National Superconducting Cyclotron Laboratory (NSCL), East Lansing, MI, USA, was measured by using the foil activation method. Several ^{115}In and ^{27}Al foils were irradiated at different positions around the target. The induced activities were counted by the HPGe detector and a personal computer multi-channel analyzer. Angular distributions of the flux are presented. The data are compared with those in the literature.

Introduction

When an energetic beam hits a target, different types of radiation such as gammas and neutrons come out with different energies as a result of the fragmentation or break-up process[1]. The neutron fluxes from such reactions are large. Tuyn *et al.* used a current of the order of 10^{11} ^{12}C ions per second at 86 MeV/u on an iron target with ^{115}In, ^{32}S, ^{27}Al and ^{12}C as activation detectors to measure the neutron fluxes[2]. They reported fast neutron (< 20 MeV) flux of 5×10^{9} n.cm^2/g.s.sr (normalized to the target thickness and solid angle) using ^{27}Al foil at 100 cm from 3.2 g/cm^2 Fe target, at 0º. It is expected that the neutron flux will increase using heavier and more neutron-rich beams. This is displayed in this experiment with a current of 7.3×10^{11} $^{18}O^{6+}$ ions per second at 80 MeV/u on a 1.9 g/cm^2 ^{9}Be target with ^{27}Al as activation detector too.

Activation foils are used for flux measurements because they are known for their reliability and convenience[3,4]. Unlike some detectors, activation foils need no electronics during the irradiation nor do they get disabled by high fluxes. There is no interference from other radiation, like gamma-rays. The foils respond only to neutrons, therefore neutron-induced gamma activity can be conveniently counted by a simple set-up with a high resolution detector, like a high-purity germanium (HPGe) detector, and a multichannel analyzer.

*This experiment was done in 1997 during a sabbatical leave at NSCL, USA.

Experimental Setup and Method

1. Activation Foils

In this experiment, neutrons were detected by twelve activation foils. These foils were divided into three groups, A, B and C as seen in Fig. 1a. Groups B and C have an aluminum foil and two indium foils, (see Table 1). In each group, one of the indium foils was covered with cadmium foils on both sides to absorb the thermal neutrons. Group A has six foils, five of them are put on the outside surface of a 16.5 cm × 16.5 cm cylindrical neutron moderator. These foils are an aluminum foil, two bare indium foils and two indium foils covered with cadmium foils on both sides. The sixth is an indium foil which was placed inside the moderator at its center (see Fig. 1a).

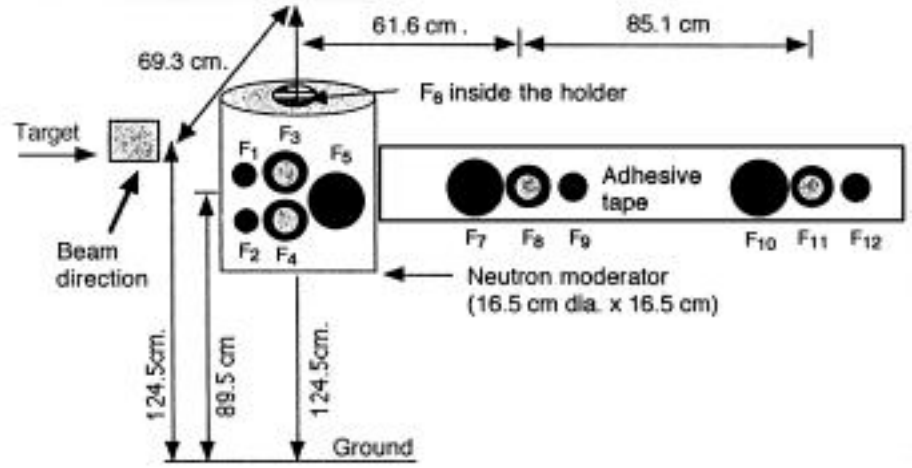

Fig. 1a. A front view of the experimental setup where foils 1-12 were irradiated (not to scale). Foils 1-5 were placed on the outside surface of the moderator under the beam line and facing the beam direction. Foil 6 was put inside the moderator at the center. Foils 7-12 were placed on an adhesive cloth tape.

TABLE 1a. The different activation foils used in the experiment.

Element of the foil	Foil number	Average mass (g)	Average diameter (cm)	Average thickness (cm)	Purity %
^{115}In	1, 2, 3, 4, 6, 9, 12 3*, 4*, 8*, 11*	0.9192 ± 0.0112	2.5400 ± 0.0500	0.0248 ± 0.0003	99.9959
^{27}Al**	5, 7, 10	14.1340 ± 0.5688	5.1	0.2650 ± 0.0093	99.00

*These are covered by cadmium foils on both sides.
**Aluminum foils were cut out from the same rod.

The location of each group relative to the other groups, the cyclotron target and the beam line is seen in Fig. 1. All the groups were placed at positions approximately 34.9 cm lower than the plane of the target and beam line such that they faced the beam. Group A was located under the beam line while groups B and C were put on an adhesive cloth tape, Fig. 1a. The distances from the target to groups locations, distances among the

groups and the angular separations relative to the beam line (taken as 0º) are explained in Table 1 and Fig. 1. As seen all the groups are in the forward direction.

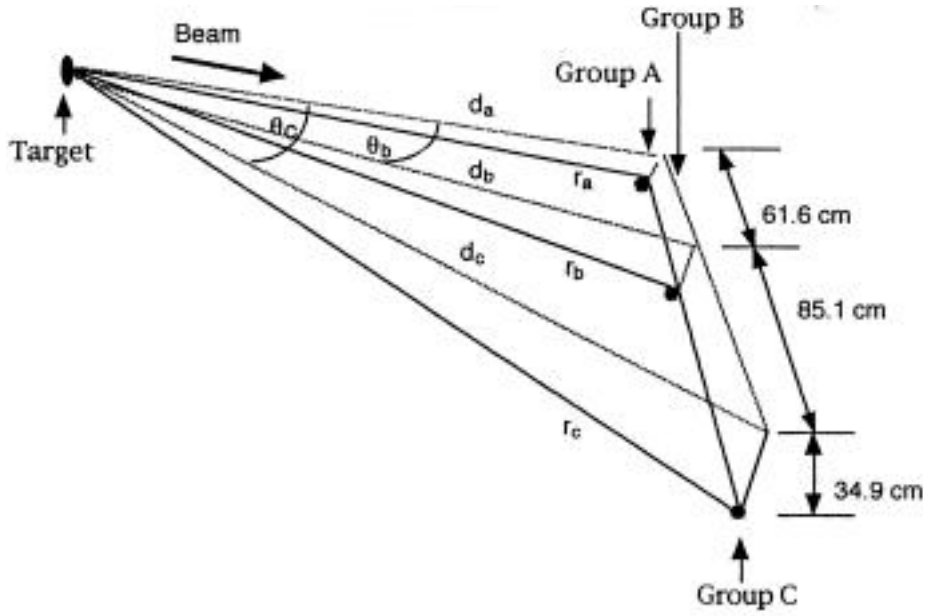

Fig. 1b. A side view of the experimental setup (see Table 1). The lines d_a, d_b, d_c, the beam line and target are in plane that makes an angle of 26.8º with a lower plane of the lines r_a, r_b and r_c. The vertical distance, between the upper plane and the position of the groups line is 34.9 cm.

TABLE 1b. The three groups of foils and their approximate angles and distances from the target.

Group	Foils in the group	Distance* from the target , d(cm) in the upper plane	Distance* from the target , r (cm) in the lower plane	The angle of each group relative to the beam line
A	F_1, F_2, F_3 F_4, F_5, F_6	69.25**	77.56**	$\theta_a = 0º$
B	F_7, F_8, F_9	92.68	99.04	$\theta_b = 41.7º$
C	F_{10}, F_{11}, F_{12}	162.21	165.93	$\theta_c = 64.7º$

*Measurements were made to the center of the group.

**These distances are measured to the center of the moderator where F_6 is located. The rest foils of the group are 8.25 cm closer to the target on d.

The average masses, diameters, thicknesses and the purities are given in Table 1a. For cadmium cover foils the values are 3.20 ± 0.23 g, 3 cm and 0.052 ± 0.004 cm respectively.

2. Irradiation of the Foils

The irradiation time of the foils at the locations described above is approximately 67 hours. The possible reactions are ^{115}In (n_{th} or n_{ep} , γ) ^{116m}In and $^{27}Al(n_f, \alpha)$ ^{24}Na where n_{th} is a thermal neutron, n_{ep} is an epithermal neutron and n_f is a fast neutron. The ab-

sorption cross-section for n_{th} is 170 ± 15 b at 0.025 eV and for n_{ep} is 3243 ± 35 b at a resonance energy of 1.457 eV. The threshold for the second reaction is 7.2 MeV with the absorption cross-section of 0.693 ± 0.045 mb[3,5]. The irradiation time when compared with the half lives of the product nuclei (for ^{116m}In, $T_{1/2}$ = 54.4 minutes and for ^{24}Na, $T_{1/2}$ = 15 hours) is long enough for In foils to reach 100% of the saturation activity and Al foils 95.5% of saturation. This can be concluded from the relation[6]

$$A = A_{sat.} (1 - e^{-\lambda t}) \quad (1)$$

where $A_{sat.}$ is the saturation activity. Since the integrated flux of the incident neutrons over the irradiation period is proportional to the induced activity in the foils[4], it becomes important to know the saturation fraction of the foil which leads to the number of the excited nuclei.

The beam from the K1200 cycloton is $^{18}O^{6+}$ on a 1.9 g/cm^2 ^{9}Be target with beam current is 700 ena(electron nanoampere) at 80 MeV/u or, therefore 7.3×10^{11} ions/s.

3. Counting the Foils.

Each foil was counted for 10 minutes (with an average dead time less than 2% for Al foils, about 24% for bare In foils and about 12% for the rest of the In foils), by an energy calibrated 75.5 mm (diameter) × 92.0 mm (long) hyperpure germanium (HPGe) detector that has an active volume of 411.67 cm^3. Each foil was counted at 5 cm from the center of the front face of the detector crystal. This counting position and the detector were well shielded by lead bricks. All foils were counted within 3 hours after the end of the irradiation.

Several gamma standard sources (^{60}Co, ^{22}Na, ^{133}Ba, ^{54}Mn, ^{57}Co, ^{109}Cd) were used for full-energy peak efficiency (Fig. 2) and energy calibration of the HPGe detector. The activity of these standard sources ranges from 1-12 μCi. The latter had a FWHM energy resolution of 4.5 keV at 1332.5 keV of ^{60}Co. Although the resolution should be better than this, the gamma peaks were well resolved as can be seen in Fig. 3. The same geometrical position relative to the HPGe detector was preserved during the different stages of the work. The absolute full-energy peak efficiency was corrected for the coincidence summing effect in the case of ^{60}Co, ^{22}Na and ^{133}Ba which are multiple-line γ sources, thus coincidence correction is relevant. On the other hand, ^{54}Mn, ^{57}Co and ^{109}Cd are single-line γ sources and don't require this correction[7]. Since summing effects depend on the square of the detector solid angle[8], the summing correction factors for this detector were calculated by scaling from correction factors of another HPGe detector with the same geometrical positions but a 1 and 10 cm from the detector[9]. The dead time during the efficiency measurement is less than 2%. The experimental efficiency data points, Fig. 2, were fitted by the equation.

$$\varepsilon = a + b\,(E)^{0.5}\,\ln E + c\,\ln(E) / E^2 + d/E^2 \quad (2)$$

where ε is the efficiency. The constants $a = 1752.21 \times 10^{-3}$, $b = -3386 \times 10^{-6}$, $c = 4941 \times 10^{-1}$ and $d = -2161.5096 \times 10^2$ are the fitting parameters. The fit goodness parameter κ^2 is 0.998. The uncertainty of about 3.1% in the experimental efficiency data points is due to the counting statistics.

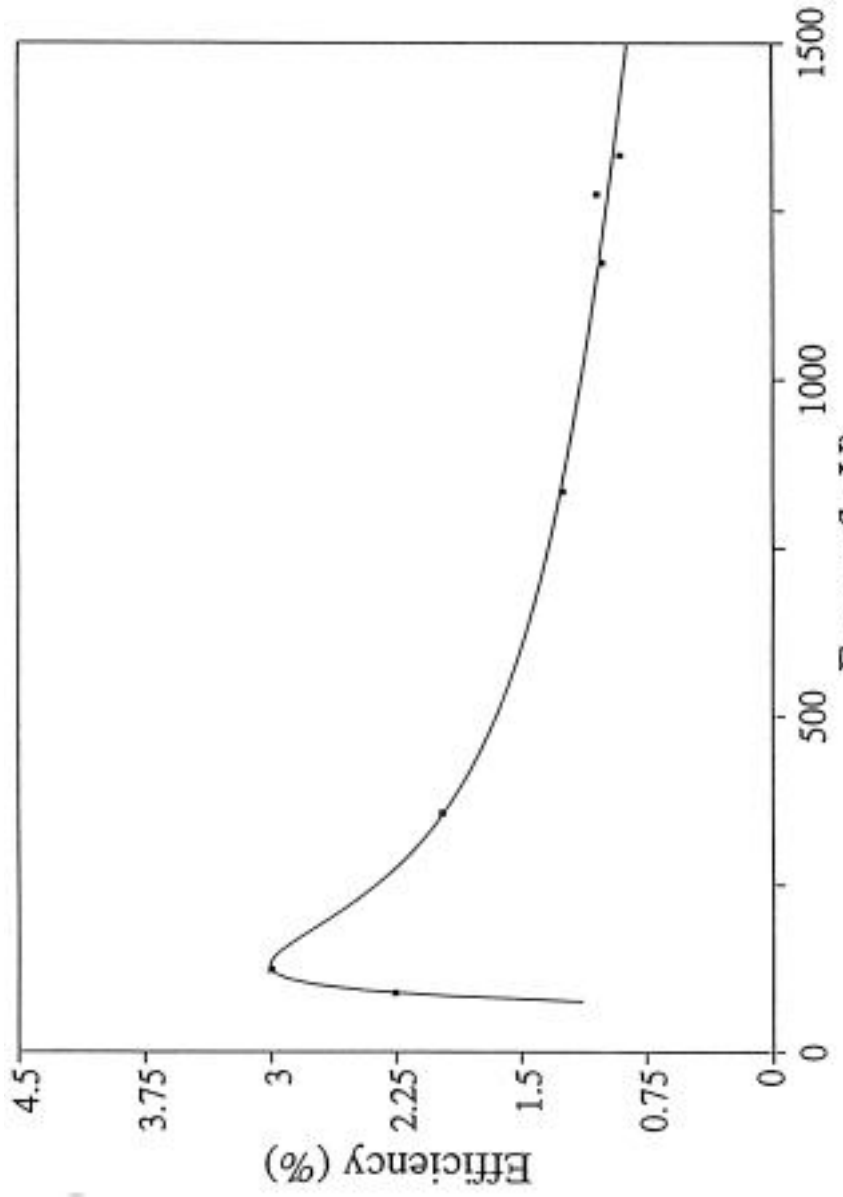

FIG. 2. The efficiency curve of the hyper pure germanium detector used in this experiment. Data points were fitted by the curve.

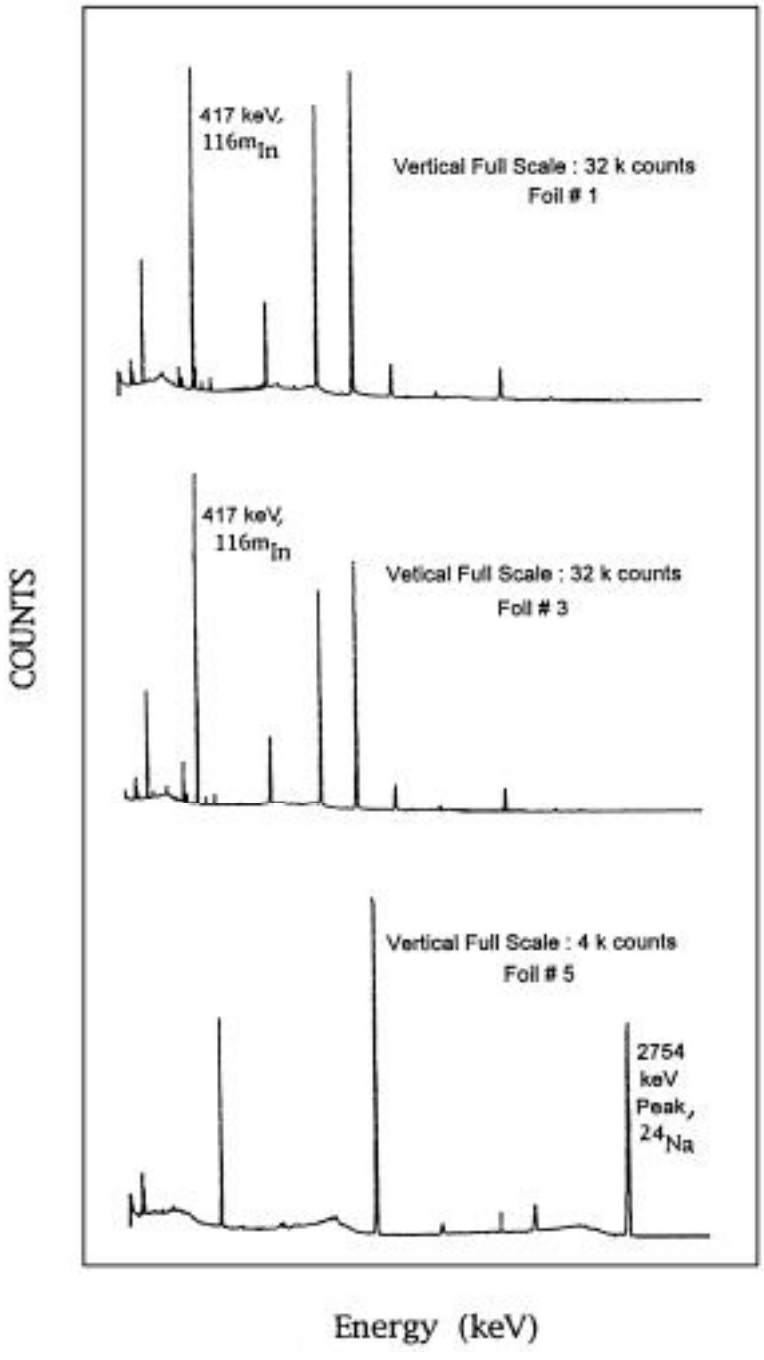

FIG. 3. The gamma ray spectra from counting: (top) the bare ^{115}In foil F_1, (middle) the cadmium covered ^{115}In foil F_3 and (bottom) the ^{27}Al foil, F_5.

Analysis and Results

Both slow or thermal ($E_n < 0.5$ eV) and intermediate or epithermal (0.5 eV < E_n < 10 keV) absorption activations follows (n, γ) reaction[3]. ^{115}In has a large neutron absorption cross-sections in the thermal and epithermal energy ranges and can be used as neutron detector for these energies. The product nucleus of the above reaction is ^{116m}In which decays by emitting several gamma lines. One of these lines, the 417 keV line with absolute intensity of 32.4%, was observed in this experiment and used for flux calculations. Unlike the thermal and epithermal neutrons, fast neutrons ($E_n > 10$ keV) are detected by threshold activation in which a nuclear particle is emitted such as (n, p), (n, n) and (n, α) reactions. In this experiment ^{27}Al foil was used to identify fast neutrons through the ^{27}Al (n, α) ^{24}Na reaction. ^{24}Na decays by emitting β^- particle with 100% to two excited states of ^{24}Mg which decays to its ground state by emitting the two γ-lines 1368 and 2754 keV. In this experiment, the induced activity of the 2754 keV line (net area of the peak) was used for fast neutron flux calculation whereas the induced activity of the 417 keV line in the Cd covered ^{115}In foil was used for the intermediate energy fast neutron flux. By subtracting the counts of the 417 keV line in the Cd- covered ^{115}In foil which was used for intermediate fast neutron flux from the counts of the 417 keV line in the bare. ^{115}In, thermal neutrons counts are determined[3]. This was done because bare ^{115}In detects both thermal and epithermal neutrons with the same reaction. These counts were corrected for background. The flux is calculated by the following equation[3]:

$$\Phi = \Delta N / [\sigma(1E\text{-}24)\, N_s SAPEB\, (\exp. - \mu_s (X_s/2))\, (\exp. - \mu_a X_a)\, (\exp. - \Sigma_n X_s)\, (\exp. - \lambda t_d)\, (1 - (\exp. - \lambda t_i))\, (1 - (\exp. - \lambda t_c))] \quad (3)$$

where

- Φ = neutron flux (n/cm^2.s)
- ΔN = number of counts during the counting time t_c in seconds.
- σ = cross section (barn).
- N_s = number of nuclei in the foils (^{115}In, ^{27}Al).
- S = saturation fraction of the foil.
- A = abundance fraction of foil.
- P = purity fraction of the foil.
- E = efficiency of the detector (HPGe) at the relevant energies of gamma.
- B = the absolute intensity of gamma line of interest.
- $\mu_s(X_s/2)$ = the total attenuation coefficient of gamma in the foils with μ_s at the relevant energies and the half thickness of the foil $X_s/2$.
- $\mu_a X_a$ = the total attenuation coefficient of gamma in air μ_a at the relevant energies and the separation between the foils and the detector X_a.
- $\Sigma_n X_s$ = the attenuation of neutrons in the foils Σ_n at the relevant energies and foil thickness (X_s).
- t_i, t_d, t_c = irradiation, decay and counting periods were the counting time was corrected for the dead time. The decay time was taken from the end of irradiation to the midpoint of the counting interval.
- λ = decay constant for the product nuclei (^{116m}In and ^{27}Al).

The flux results are listed in Table 2. It should be noticed that the flux values calculated for A, B and C groups at 1 cm from the target have approximately the same order of magnitude and they average to 3.6×10^{11} n/cm^2.s for thermal, 4.3×10^{10} n/cm^2.s for intermediate and 2.9×10^{15} n/cm^2.s for fast. The uncertainty in these values is about 9.4% for thermal, 3.4% for intermediate and 7.7% for fast neutrons. This uncertainty is due to counting statistics, cross-sections and efficiency. Since the induced activity (of 2754 keV ^{24}Na peak here) is proportional to the fast neutron flux with energies above the threshold[3], this flux was calculated using the cross-section of 0.693 mb at the threshold of 7.2 MeV. It is not known from what depth in the foil γ-ray was emitted, therefore half the foil thickness was used to correct for the self absorption. However, this correction is only about 2.5% which is smaller than the uncertainty in the flux values. The correction for neutron attenuation in ^{115}In was neglected because neutrons will be absorbed in these foils due to their low energy. In addition to that, the thickness of ^{115}In foils is very small (see Table 1a). This wasn't the case of the relatively thicker ^{27}Al foils which interact with fast neutrons.

TABLE 2. The neutron fluxes at the different locations in this experiment*.

Group		Neutron energy	At the sample position	At 1 cm from target position**
A	Flux (Neutrons / cm^2.s)	Thermal Intermediate Fast	5.9E8 7.4E7 1.4E13	2.3E11 2.9E10 5.4E15
	$\frac{Neutrons / cm^2}{\text{Beam particle}}$	Thermal Intermediate Fast	8.1E-4 1.0E-4 1.9E1	3.2E-1 4.0E-2 7.4E3
B	Flux (Neutrons / cm^2.s)	Thermal Intermediate Fast	3.3E8 4.0E7 2.9E12	2.6E11 3.1E10 2.3E15
	$\frac{Neutrons / cm^2}{\text{Beam Particle}}$	Thermal Intermediate Fast	1.5E-4 5.4E-5 4.0EO	1.2E-1 4.3E-2 3.1E3
C	Flux (Neutrons / cm^2.s)	Thermal Intermediate fast	2.7E8 3.2E7 4.9E11	6.0E11 7.1E10 1.1E15
	$\frac{Neutrons / cm^2}{\text{Beam particle}}$	Thermal Intermediate Fast	3.8E-4 4.4E-5 6.8E-1	8.3E-1 9.7E-2 1.5E3

*80 MeV/u $^{18}O^{6+}$ beam on an 1.9 g/cm^2 ^{9}Be target.
**These values are calculated from the measured values at the sample position.

Being inside a neutron moderator, F_6 (^{115}In foil) detected thermalized fast neutrons. The energy response of the moderator is essentially uniform from 20 keV to 20 MeV[4]. The fast flux at 1 cm from the target position measured by F_6 is 1.9153×10^{11} n/cm^2.s. This is very much less than the other value of the same neutron group which was measured by ^{27}Al foil, F_5. This can be justified by considering the difference of the reactions in the

two cases. The reaction in ^{27}Al is insensitive for neutrons with En < 7.2 MeV whereas F_6 is very sensitive to all fast neutrons that were thermalized by the moderator. F_6 is also about 7 cm farther from the target and was located behind all the foils which were positioned on the moderator surface. This may led to degrading the flux at the F_6 location.

The angular distribution a of the flux at the same radial distance of 70.32 cm from the target is presented in Fig. 4. It should be noticed that the flux values for each type of neutron differ by a factor of 10 at the most.

Conclusion

The data and the results of this experiment show that the neutron flux measured in this experiment correspond to a flux of about of 10^{11} n/cm^2.s for thermal neutrons, 10^{10} n/cm^2.s for intermediate energy neutrons and 10^{15} n/cm^2.s for fast neutrons at 1 cm from the target. The 0º fast neutron flux calculated at 100 cm and normalized to 1.9 g/cm^2 ^{9}Be target thickness is 3.6×10^{16} n.cm^2/g.s.sr, which is much higher than Tuyn's value of 5×10^9 n.cm^2/g.s.sr[2]. This experiment was done at comparable beam intensity and energy per beam ion, to those of Tuyn *et al.* Therefore this difference can be justified, in part, by the heavier, more neutron-rich beam that was used in this experiment. Also, different cross-sections $\sigma(n_f$ on $^{27}Al)$ were used. Tuyn *et al.* used $\sigma(n_f$ on $^{27}Al)$ of 63 mb which is about 10^2 larger than $\sigma(n_f$ on $^{27}Al)$ of 0.693 mb used in this experiment. Using $\sigma(n_f$ on $^{27}Al)$ of 63 mb, the flux will be 4×10^{14} n.cm^2/g.s.sr.

Due to the induced activities in near by objects such shielding walls, vacuum chambers and slits when struck by the beam, neutron flux and any other secondary radiation (α, β and γ), this data is relevance to laboratories for the safety of workers and experiment electronics[10]. Depending on the half lives of the different elements formed, the induced activities may last for many hours or days after the shut down of the beam.

The application of the foil activation detection system reflects their simplicity and practicality. This suggests that these types of measurements should be done more frequently during the laboratory approved experiments using different beams and setups.

References

[1] **Charvet, J.L., Duchene, G., Joly, S., Magnago, C., Morjean, M., Patin, Y., Pranal, Y., Sinopoli, L., Uzureau, J.L., Billerey, R., Chambon, B., Chbihi, A., Chevarier, A., Chevarier, N., Drain, D., Pastor, C., Stern, M., Peghaire, A.,** *Physics Letters B,* **189**(4): 388 (1987).

[2] **Tuyn, J.W.N., Deltenre, C., Lamberet, C.** and **Roubaud, G.,** *Proc. 6th Int. Cong. IRPA, Berlin,* 673 (1984).

[3] **Scientific Staff,** *Activation Foil Manual,* Reactor Experiment Inc., California, USA (1965).

[4] **Scientific Staff,** *Neutron Flux Integrator,* Reactor Experiment Inc., California, USA (1965).

[5] **Erdtmann, G.,** *The Neutron Activation Tables,* vol. **6,** Verlag-Chemie, New York (1976).

[6] **Lamarsh, J.R.,** *Introduction to Nuclear Engineering,* Addison-Wesley, third edition (1977).

[7] **Quittner, P.,** *Gamma-Ray Spectroscopy,* second edition, Hilger, p. 98 (1973).

[8] **Ramos-Lerate, I., Barrera, M., Ligero, R.A.** and **Casas-Ruiz, M.,** *Nuclear Instruments and Methods,* **A395:** 202 (1997).

[9] **Aksoy, A.,** *Journal of Radioanalytical and Nuclear Chemistry,* **169**(2): 463 (1993).

[10] **Radiation Safety Manual,** National Superconducting Cyclotron Laboratory, East Lansing, Michigan, USA (1996).

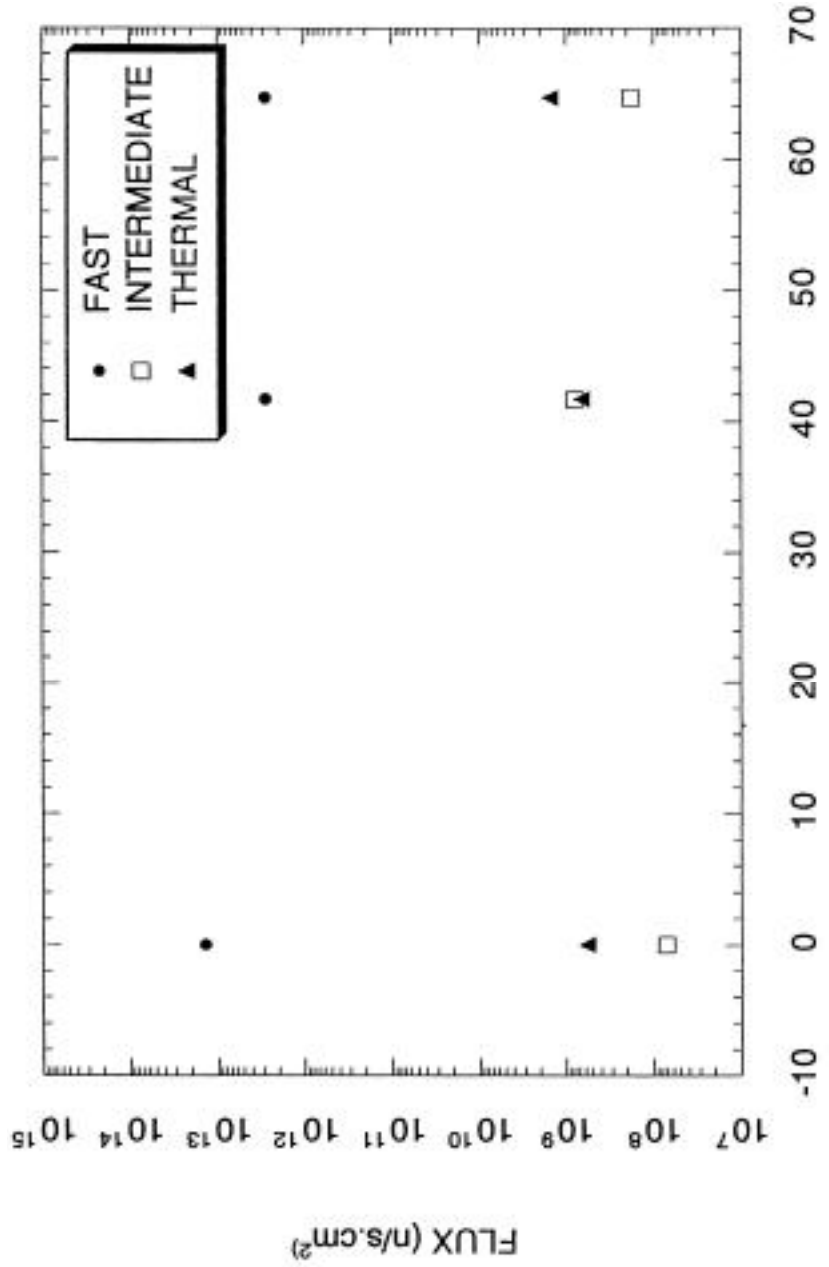

FIG. 4. The angular distribution of the flux at the foil locations for the thermal, intermediate and fast neutrons.

قياس الفيض النيوتروني في المعمل الوطني للمعجل الدائري فائق التوصيل K1200 باستخدام التفاعل النـووي لشعــاع أيوني من $^{18}O^{+6}$ معجل بطاقة قدرها ٨٠ ميغا الكترون فولت لوحدة الكتلة الذرية ، مع الهدف ^{9}Be

سالم علي سالم شاهين

قسم الفيزياء ، كلية العــلوم ، جامعة الملك عبد العزيز

جـــــــدة – المملكة العربية السعودية

المستخلص . تم قياس الفيض النيوتروني قريباً من هدف المعجل الدائري فائق التوصيل K1200 في المعمل الوطني بمدينةايست لانسنج بولاية ميشجان في الولايا المتحدة الأمريكية باستخــدام التنشيط الاشعــاعي لعـدد من صفائح ^{27}Al و ^{115}In وضعت في مـواقع متعددة حـول هدف المعجل . ولقـد حسب النشاط الاشعاعي الناتج عن التشعيع باستخدام كاشف جرمانيوم بالغ النقاوة ، وحاسب شخصي يحوي محلل متعدد القنوا . كما يعرض التوزيع الزاوي للفيض ومقارنة نتائج هذا البحث بنتائج أبحاث أخرى .